NO laser-induced fluorescence studies for the application of single-shot two-line thermometry to HEG

M. Wollenhaupt, M. Rosenhauer, T. Müller, J. Jourdan, J. Scholz, S. Hartung, W.H. Beck

DLR Institute of Fluid Mechanics, Bunsenstr. 10, D-37073 Göttingen, Germany

Abstract: Experiments in a heated cell for the application of single pulse two-line thermometry to HEG are described. Simultaneous measurements of NO excitation/fluorescence spectra, and infrared amplified spontaneous emission spectra are used for line identification and analysis of deexcitation processes. Measurement uncertainties arising from pulse-to-pulse laser fluctuations are studied and suitable correction methods are discussed. The influence of laser and fluorescence (re-) absorption, saturation effects and energy transfer on fluorescence ratios is described. Results of LIF experiments on HEG in the shock layer of a sphere are presented along with measurements of the vibrational temperature in the free stream.

Key words: Shock tunnel, Laser-induced fluorescence, Nitric Oxide, HEG, NO spectroscopy

1. Introduction

Nitric oxide (NO) LIF studies at 193 nm using two ArF excimer lasers are being carried out with the aim of determining rotational and vibrational temperatures and NO densities both in the free stream and also behind shock waves in front of models in HEG. Due to the short test time (∼1 ms), two-line thermometry (TLT) using two-laser single-shot LIF is applied. With this method the population of two quantum states of the NO molecule is probed by detection of the corresponding laser-excited fluorescence. Using broadband detection, the fluorescence signal S in the limit of linear LIF is given by (Hanson et al. (1990))

$$S \;=\; B\,E\,g\,N\,f_B\,q_F\,\Omega/4\pi\,\eta\,V, \qquad (1)$$

where N is the NO number density, f_B the Boltzmann fraction, B the Einstein-coefficient for absorption, E the laser energy, g the spectral overlap integral, q_F the quantum yield for fluorescence, $\Omega/4\pi$ the solid angle, η the optical sensitivity and V the measurement volume. Temperatures are to be determined from the ratio R of the fluorescence intensities captured by two camera systems:

$$R := \frac{S_1/E_1 g_1}{S_2/E_2 g_2} \propto e^{-\frac{\Delta E}{kT}} = e^{-\frac{\Delta E_{vib}}{kT_{vib}}}\, e^{-\frac{\Delta E_{rot}}{kT_{rot}}}. \qquad (2)$$

Equation 2 shows that the sensitivity for the determination of rotational and vibrational temperatures is dependent on the energy differences ΔE_{rot} and ΔE_{vib} of the two lower rovibrational states. With this criterion in mind, suitable excitation lines for the application of TLT to HEG have been identified. The fluorescence signal S is influenced by intensity and spectral pulse-to-pulse fluctuations of the laser ($g\,E$). Therefore, an appropriate signal correction of fluorescence ratios R is essential for single-pulse measurements in impulse facilities such as HEG. The effects of two correction schemes on the precision of single-pulse temperature measurements are discussed. In order to investigate sources of systematic errors, fluorescence ratios R have been measured in a cell as a function of temperature and number density. The influence of fluorescence reabsorption and laser absorption, saturation and energy transfer on fluorescence ratios is analyzed.

2. NO spectroscopy

To identify suitable excitation lines for the determination of vibrational and rotational temperatures in HEG, excitation/fluorescence spectra of NO at 193 nm were measured in a heated cell. The analysis of these spectra resulted in a complete assignment of all the observed transitions (Beck et al. (1996)). The simultaneous detection of fluorescence and collimated infrared radiation showed that stimulated emission between excited states provides an additional deexcitation pathway.

2.1. Experimental arrangement

The experimental arrangement for spectroscopic measurements is shown in Fig. 1. The output of a tunable ArF excimer laser (51580 – 51850 cm^{-1}, maximum spectral intensity 10^6 J/s cm^{-1} cm^2) is directed into a heated cell (300 – 1300 K) containing NO gas at a number density of 10^{15} – 10^{17} cm^{-3}. 5% of the laser energy is deflected to an energy monitor. The NO fluorescence is detected perpendicular to the laser beam spectrally resolved (180 – 280 nm) using two OMA with low and high spectral resolution (see UV-fluorescence spectra in Fig. 1). By excitation to the NO $D^2\Sigma^+(v'=0)$ state, a population inversion between the excited $D^2\Sigma^+$ and $A^2\Sigma^+$ levels can be established. Photons $D^2\Sigma^+(v'=0) \rightarrow A^2\Sigma^+(v'=0)$ emitted spontaneously in the direction of the excitation volume can be amplified by stimulated emission (ASE), giving rise to an infra-red coherent signal beam collinear to the laser beam. This IR-ASE radiation in the forward direction is observed spectrally

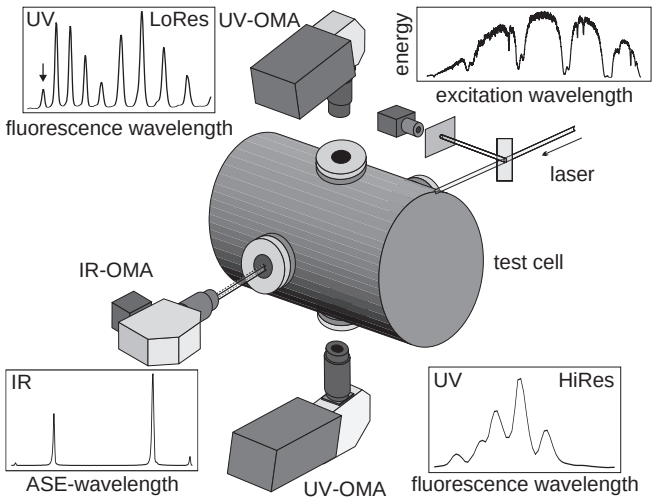

Figure 1. Experimental arrangement for spectroscopic measurements.

resolved with a modified OMA (1080 – 1120 nm). By tuning the laser, the energy, UV-fluorescence and IR-ASE can be measured as a function of the excitation wavelength.

2.2. Results

Figure 2 shows an excerpt of the NO-excitation spectrum with (1) UV and (2) IR detection. Comparison with simulated $\varepsilon(0,1)$ excitation spectra reveals that ASE-radiation is only observed when the NO $D^2\Sigma^+(v'=0)$ state is excited. When the density of excited molecules is too low, no ASE-radiation is observed, i.e. there is an excitation threshold for stimulated emission. Consequently, the infrared excitation spectrum has a higher resolution (see arrows in Fig. 2). The observed IR spectra (see Fig. 1) are well described by the allowed $D^2\Sigma^+(v'=0) \rightarrow A^2\Sigma^+(v'=0)$ transitions at line positions determined by Amiot (1982).

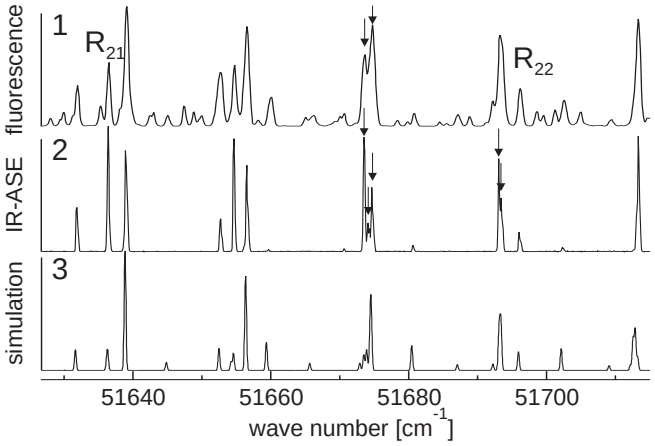

Figure 2. Excerpt of the NO excitation spectrum with (1) UV-fluorescence (200-300 nm), (2) infrared ASE-radiation and (3) simulated $\varepsilon(0,1)$ excitation spectrum.

Since stimulated emission between excited states introduces an efficient process for depopulating the laser-excited state (Westblom et al. (1990)), the influence on LIF-intensities for temperature determination is investigated in section 3. The excitation lines for use on HEG are: $\varepsilon(0,1)$ $R_{22}(27.5)$ and $\varepsilon(0,1)$ $R_{21}(17.5)$+$P_{11}(35.5)$ (ΔE_{Rot} = 912 cm^{-1}) for determination of rotational temperatures, and $\gamma(3,0)$ $R_{11}(45.5)$+$\gamma(4,1)$ $R_{11}(27.5)$ (ΔE_{Rot} = 2231 cm^{-1}, ΔE_{Vib} = -1876 cm^{-1}) for vibrational temperatures.

3. Two-line thermometry

Temperatures are determined by the observed fluorescence ratios (see Eq. 2), which are expected to be a simple function of temperature, independent of the NO number density. Fluorescence ratios are influenced by pulse-to-pulse laser fluctuations and systematic effects such as absorption and energy transfer. For this reason, single-pulse measurements are analyzed in section 3.2. and averaged fluorescence ratios are investigated in section 3.3.

3.1. Experimental arrangement

The set-up for the experiments testing TLT is shown in Fig. 3. The experimental parameters are described in section 2.1. In this set-up, the test cell is used to measure NO fluorescence as a function of temperature and density. The reference cell is used for an intensity correction at constant gas conditions (600 K, 6·10^{16} cm^{-3}). Using a 50% beam splitter, NO molecules in both cells are excited with identical laser energies. The NO fluorescence is detected with two OMA; the laser energy is measured with two energy monitors. At each gas condition the lasers are tuned to the NO transitions $\varepsilon(0,1)$

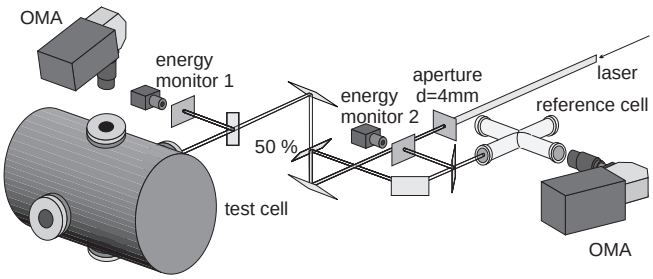

Figure 3. Experimental arrangement for testing two-line thermometry.

$R_{22}(27.5)$ and $\varepsilon(0,1)R_{21}(17.5)$+$P_{11}(35.5)$. Using these transitions the single-pulse fluorescence and laser energy was measured for 140 laser pulses.

3.2. Single pulse measurements

Figure 4 shows the relative deviation δ from the average for the uncorrected measured fluorescence (1), the laser energy corrected fluorescence (2) and the fluores-

cence corrected by the signal in the reference cell (3). Fluorescence or energy correction leads to a reduction of the standard deviation by a factor of about 3 or 1.5, respectively, i.e. the fluorescence correction provides a significant improvement over the usual energy correction. There is evidence to show that saturation effects and spectral pulse-to-pulse fluctuations of the laser which are not considered by the energy measurement lead to an improved correction using a second heated cell (Wollenhaupt (1997)). In order to determine the influence of the correction procedure on the precision of

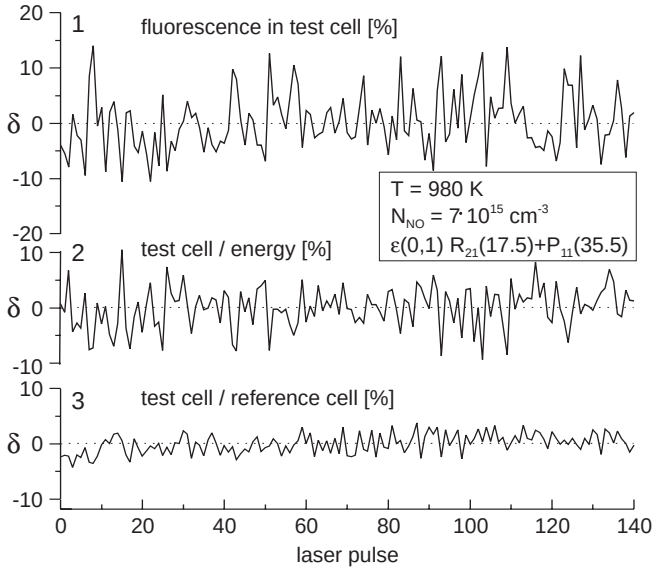

Figure 4. (1) Pulse-to-pulse fluctuations of the fluorescence, (2) corrections with laser energy and (3) corrections with fluorescence in reference cell.

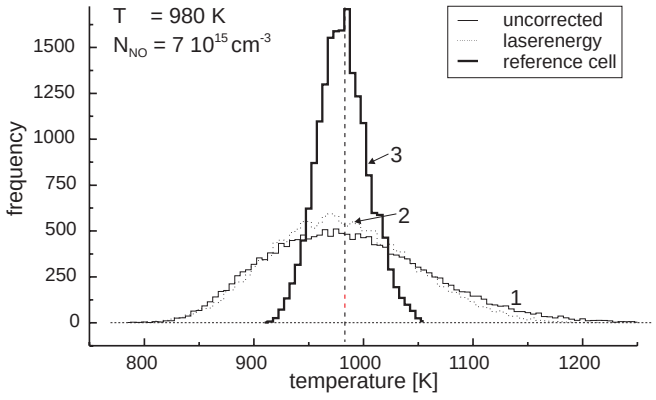

Figure 5. Temperature histogram comparing uncorrected and corrected fluorescence ratios.

single pulse temperature determination, the signals of 140 single pulse fluorescence measurements for both excitation lines were combined to yield 140^2 temperature values. Figure 5 shows the temperature histogram of the single-pulse temperature measurement without correction (1), with an energy correction (2), and with a reference cell correction (3). The standard deviation of the temperature distribution is reduced by a factor of 3 for the reference cell correction, whereas the error is not reduced by an energy correction.

3.3. Fluorescence ratios

Besides the error of the single-pulse measurement, sources of systematic errors in the TLT-method were investigated. For this purpose, the fluorescence after the excitation of the above mentioned lines was measured as a function of temperature and NO number density. Fluorescence ratios $R{:=}S(R_{22})/S(R_{21})$ were calculated for the $\varepsilon(0, v'' = 3, 4)$ fluorescence (R^D) and the $\gamma(0, v'' = 3, 4)$ cascade fluorescence (R^D). R^{DA} describes the energy transfer ratio $D^2\Sigma^+ \rightarrow A^2\Sigma^+$ for both lines. Even at constant temperature, the fluorescence ratios exhibited considerable variations with the NO number density. The analysis of the NO fluorescence spectra shows the influence of fluorescence reabsorption (trapping) and radiative and non radiative energy transfer. Moreover, the observed fluorescence ratios are influenced by the saturation of NO transitions and laser absorption.

3.3.1. Reabsorption of fluorescence

Figure 6 shows the observed transmission of $\varepsilon(0, v'' = 1, 2)$ fluorescence as a function of NO pressure at 860, 1050 and 1250 K and a comparison to calculated values. Since the reabsorption is dependent on the thermal population and the Einstein-B-coefficient, it may be different for both lines and thus alter the fluorescence ratios. In order to eliminate the influence of fluorescence reabsorption even at higher pressures, only the $\varepsilon(0, v'' = 3, 4)$ fluorescence transitions are used for data evaluation.

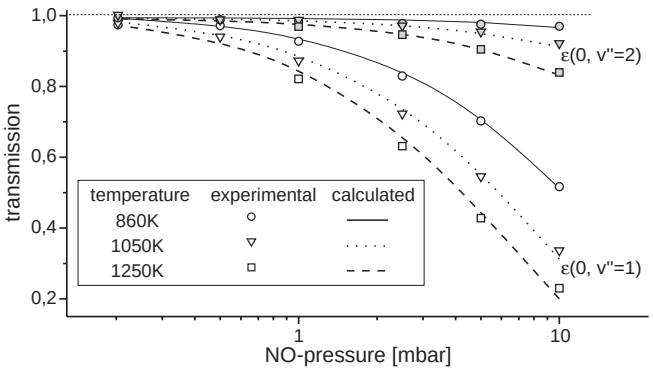

Figure 6. Transmission of $\varepsilon(0, v'')$-fluorescence as a function of pressure.

3.3.2. Quenching and laser absorption

The intensity of the NO $\varepsilon(0, v'' = 3, 4)$ fluorescence as a function of the NO number density is shown in Fig. 7

for both excitation lines. Calculated number densities of NO in the HEG free stream for conditions I - VI are shown for comparison. For low number densities, the fluorescence is well described by the number density multiplied by the quantum yield $q_F = A/(A+Q)$ (see dashed line in Fig. 7). At higher number densities, laser absorption is no longer negligible. If laser transmission $\Theta(f_B(T), N, B)$ is taken into account, a good agreement between measurements and calculations can be obtained (see solid line in Fig. 7). For quantitative interpretation of fluorescence ratios, measured intensities are corrected for absorption, since laser absorption is different for both lines.

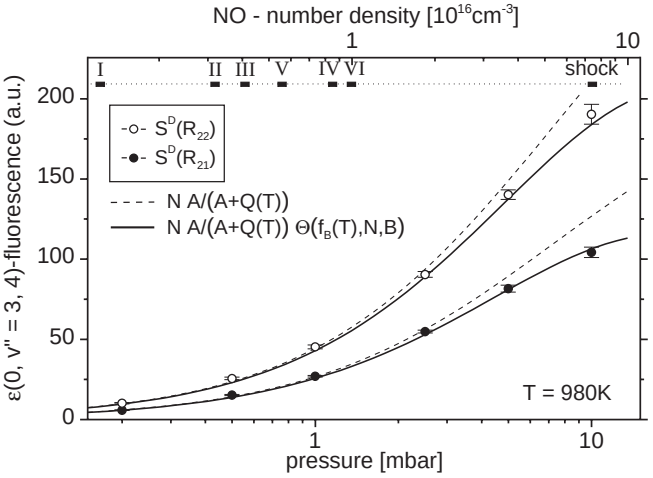

Figure 7. NO fluorescence versus number density.

3.3.3. Saturation

At very high laser power densities, NO transitions having strong Einstein-B-coefficients are saturated. As a consequence, the fluorescence signal no longer increases linearly with increasing laser spectral intensity, as is shown in Fig. 8. At laser energies used in the experiments, both transitions are partially saturated. Due to the different Einstein-B-coefficients ($\varepsilon(0,1)$ $R_{22}(27.5)$: 1000 cm/J, $\varepsilon(0,1)$ $R_{21}(17.5)$: 400 cm/J) the degree of saturation is different for both lines. This results in a laser power density dependence of the fluorescence ratios (see Fig. 8). Therefore, the heated cell tests were carried out at constant laser energy, thus avoiding a change in saturation. If saturation effects play a significant role, fluorescence ratios cannot easily be converted into population ratios, i.e. fluorescence ratios have to be calibrated for a temperature determination. For this reason, it may be advantageous to de-focus the laser beam in order to facilitate data evaluation. Additionally, the fluorescence intensity may be increased by optical integration over the enlarged fluorescence volume and avoiding saturation, as was demonstrated with the sphere experiments

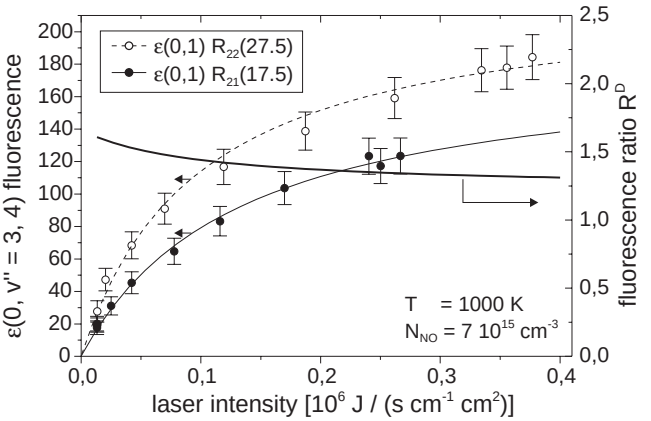

Figure 8. Saturation of the excitation transitions $\varepsilon(0,1)$ $R_{22}(27.5)$ and $\varepsilon(0,1)$ $R_{21}(17.5)$+$P_{11}(35.5)$.

on HEG (see section 4.2.).

3.3.4. Energy transfer

LIF signals are dependent on the quantum yield for fluorescence. For temperature determination, fluorescence ratios are used to eliminate the influence of deexcitation processes. If the fluorescence quantum yields for both excitations are not equal, fluorescence ratios are altered significantly. For this reason the energy transfer $D^2\Sigma^+(v'=0) \rightarrow A^2\Sigma^+(v'=0)$ was investigated for both excitation lines. At sufficiently high NO number densities, the energy transfer rates are equal for both excited states (see Fig. 9, right). At lower number densities, the excited states show a significant difference in energy transfer (see Fig. 9, left), i.e. the depopulation process for the $R_{21}(17.5)$ line is twice as efficient as for the $R_{22}(27.5)$ line. As a consequence, the fluorescence intensity of the $R_{21}(17.5)$ line is reduced, leading to an

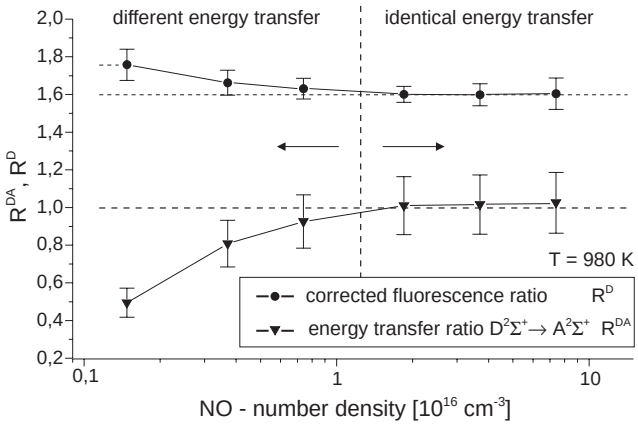

Figure 9. Influence of energy transfer on fluorescence ratios.

increase of the fluorescence ratios. The analysis of the temperature and density dependence of fluorescence ra-

tios shows that their behavior at low densities can be explained by energy transfer through ASE between the excited states $D^2\Sigma^+(v'=0) \rightarrow A^2\Sigma^+(v'=0)$. Figure 10

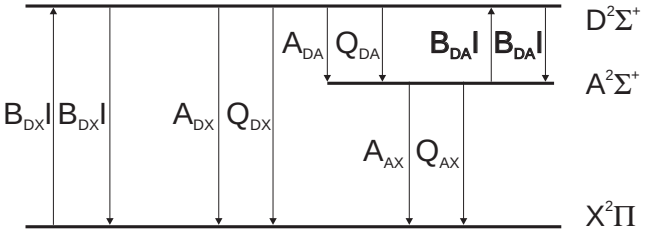

Figure 10. Three-level-system including energy-transfer by stimulated emission in the excited states.

shows a three-level system for the description of the NO $\varepsilon(0, v'')$ fluorescence and the $\gamma(0, v'')$ cascade fluorescence. If stimulated transitions between excited states are considered, it is obvious that the onset of the energy transfer through stimulated emission is dependent on the excited number density of NO molecules. This means that the population inversion between the excited states is (1) different for both lines, (2) dependent on number density, and (3) dependent on laser-energy density.

3.3.5. Temperature dependence

The temperature dependence of the $\varepsilon(0, v''=3, 4)$ fluorescence ratios R^D and the $\gamma(0, v''=3, 4)$ cascade fluorescence ratios R^A is shown in Fig. 11. At lower tem-

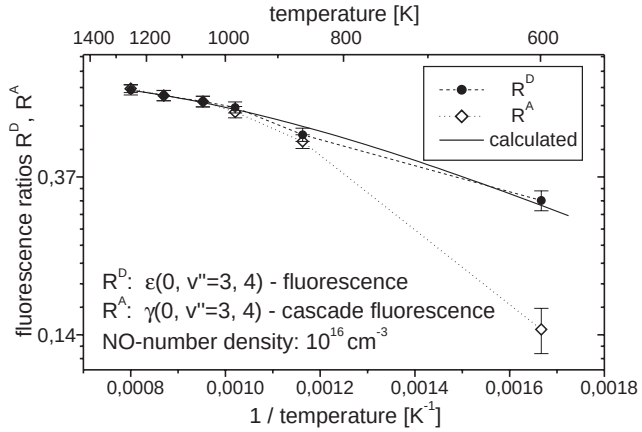

Figure 11. Boltzmann plot of the fluorescence ratios.

peratures, the ratios R^A and R^D are completely different. This is due to the different energy transfer for both excitation lines. Whereas the R_{22}-excited level is still below the threshold for stimulated emission leading to low energy transfer rates, the R_{21}-excited level is sufficiently populated for rapid energy transfer to the $A^2\Sigma^+$ state. At higher temperatures, R^D and R^A are identical. With increasing temperature, the fluorescence ratios become less temperature sensitive, showing the influence of the interfering $P_{11}(35.5)$ transition. Comparison of the calculated population ratio of the NO $X^2\Pi(v''=1, J''=27.5, F_2)$ to the $X^2\Pi(v''=1, J''=17.5, F_1)$ + $X^2\Pi(v''=1, J''=35.5, F_1)$ states gives a good agreement with measured fluorescence ratios R^D.

3.4. Consequences for HEG

From these results it can be concluded that the lines presently used at HEG are suitable for temperature determination if the temperature is below 1000 K and narrowband detection $\varepsilon(0, v''=3, 4)$ is used. Moreover, a reduction of the laser energy density allows for measurements in the weak excitation limit, facilitating the data evaluation and reducing the influence of ASE on the fluorescence ratios.

4. Measurements on HEG

4.1. Vibrational temperatures

Calculations of HEG free stream conditions predict vibrational temperatures T_{vib} much higher than rotational temperatures T_{rot} (Hannemann (1995) and Walpot (1997)). To investigate the vibrational temperature in HEG free stream a single laser excitation scheme consisting of two rovibronic transitions in the $\gamma(3, 0)$ and $\gamma(4, 1)$ bands coinciding within the laser bandwidth has been developed and applied to HEG. By calibration in a heated cell, the population ratio of both lower states can be extracted from the observed fluorescence spectrum. Since the quantum states $X^2\Pi(v''=1, J''=27.5, F_1)$ and $X^2\Pi(v''=0, J''=45.5, F_1)$ have different vibrational and rotational energies E_{vib} and E_{rot}, the population ratio is considered as a function of T_{vib} and T_{rot} (see Fig. 12). Fluorescence spectra corresponding to the

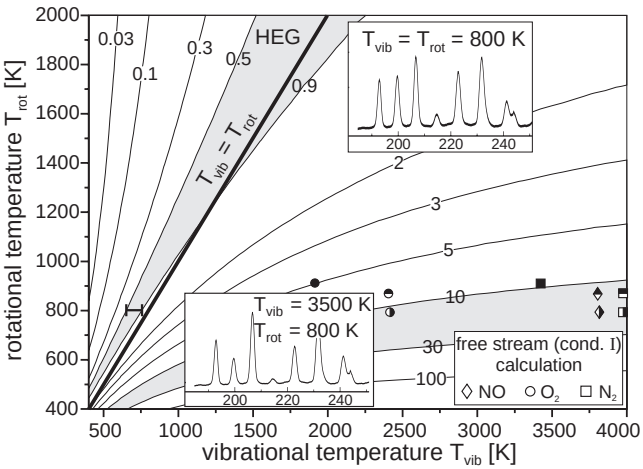

Figure 12. Population ratio of the quantum states $X^2\Pi(v''=1, J''=27.5, F_1)$ and $X^2\Pi(v''=0, J''=45.5, F_1)$ as function of T_{vib} and T_{rot}.

nonequilibrium case $T_{vib} \gg T_{rot}$ predicted by calculations and to the equilibrium case $T_{vib} = T_{rot}$ are also

shown in Fig. 12. The population ratio as measured in HEG is depicted as a grey area in Fig. 12. From this result it is concluded that the NO molecules in the HEG free stream are in a state not far removed from thermal equilibrium. However, this interpretation is only valid under the assumption of a Boltzmann distribution among all the vibrational and rotational states.

4.2. LIF behind the bow shock of a sphere

In earlier studies at HEG, no NO-LIF signals could be obtained behind strong shocks (Beck et al. (1996)). Using a refined experimental set-up (see Fig. 13), the LIF/luminosity ratio could be increased by: (1) use of a 3-d model (sphere), which provides a shorter optical integration path for the luminosity, (2) excitation of a strong group of NO-transitions, (3) use of extremely short camera gates (5-10 ns) to further suppress the intense luminosity, and (4) avoiding saturation at a constant laser energy by de-focussing the laser beams, i.e. reducing the energy density and thus increasing the LIF signal. The result, as shown in Fig. 13, is the first observation of LIF signals in the shock layer in HEG at temperatures over 6000 K.

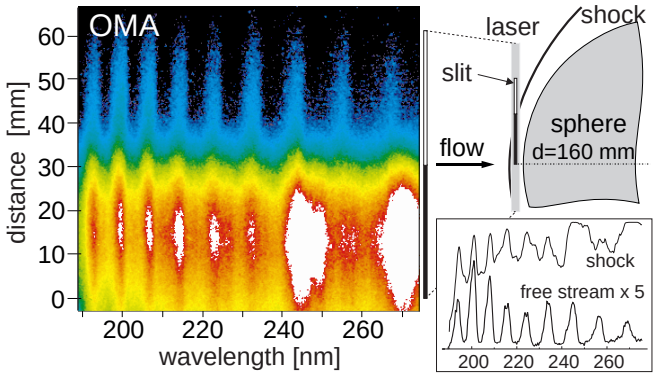

Figure 13. Experimental set-up (right) and OMA image of the fluorescence in the free stream and the shock layer (left) and corresponding spectra (right bottom).

5. Conclusions and further work

Further experiments in HEG are planned (starting with free stream) in order to determine rotational temperatures with higher accuracy using refined strategies to avoid saturation, minimize the influence of ASE, laser absorption and fluorescence reabsorption. The efficiency of the single-pulse fluctuation corrections will be increased by the use of similar measurement conditions in the reference cell and HEG free stream (laser energy and gas temperature). Temperature measurements behind shocks at temperatures T >1000 K require excitation lines with larger energy separation. For quantitative modelling of the ASE process, measurements of LIF and ASE-radiation as functions of laser intensity, NO number density, and temperature are necessary.

Acknowledgement. The authors would like to thank U. Frenzel and J. Lenz for technical assistance with laser and tunnel operation. The financial support of the ESA through CNES is gratefully acknowledged.

References

Amiot C (1982) Fourier Transform Spectrometry of the $D^2\Sigma^+$-$A^2\Sigma^+$, $E^2\Sigma^+$-$D^2\Sigma^+$ and $E^2\Sigma^+$-$D^2\Sigma^+$ Systems of Nitric Oxide. Physica Scripta 26:422–438

Beck WH, Wollenhaupt M, Rosenhauer M, Müller T, Jourdan J (1996) Status of the Development and Implementation of Optical Spectroscopic Techniques on the DLR High Enthalpy Shock Tunnel HEG. AIAA 96-2221

Hannemann K(1987) Computation of the Flow in Hypersonic Windtunnel Nozzles. DLR-IB 223-95 A47

Hanson RK, Seitzman JM, Paul PH(1990) Planar Laser-Fluorescence Imaging of Combustion Gases. Appl. Phys. B 50:441–454

Westblom U, Agrup S, Aldén M, Hertz HM, Goldsmith JEM (1990) Properties of Laser-Induced Stimulated Emission for Diagnostic Purposes. Appl. Phys. B 50:487–497

Walpot LMG (1997) One dimensional calculations for condition 1-2-3. Private communication

Wollenhaupt M (1997) Einzelpuls Zwei-Linien-Thermometrie mit planarer laserinduzierter Fluoreszenz an NO-Molekülen in Hochenthalpieströmungen. PhD Thesis, Fakultät für Physik der Universität Bielefeld